

Interface degradation and field screening mechanism behind bipolar-cycling fatigue in ferroelectric capacitors

Cite as: APL Mater. 9, 021113 (2021); <https://doi.org/10.1063/5.0038719>

Submitted: 25 November 2020 . Accepted: 06 January 2021 . Published Online: 09 February 2021

M. T. Do,  N. Gauquelin,  M. D. Nguyen, F. Blom,  J. Verbeeck,  G. Koster,  E. P. Houwman, and  G. Rijnders

COLLECTIONS

Paper published as part of the special topic on [100 Years of Ferroelectricity - a Celebration](#)



View Online



Export Citation



CrossMark

ARTICLES YOU MAY BE INTERESTED IN

[Ferroelectric field effect transistors: Progress and perspective](#)

APL Materials **9**, 021102 (2021); <https://doi.org/10.1063/5.0035515>

[Next generation ferroelectric materials for semiconductor process integration and their applications](#)

Journal of Applied Physics **129**, 100901 (2021); <https://doi.org/10.1063/5.0037617>

[Epitaxial ferroelectric oxides on silicon with perspectives for future device applications](#)

APL Materials **9**, 040701 (2021); <https://doi.org/10.1063/5.0039161>



AVS[®] 2021 International Twitter Poster Competition
JUNE 2-3, 2021
Register at www.avs.org/posters2021 • [#AVSPosters2021](https://twitter.com/AVSPosters2021)

Interface degradation and field screening mechanism behind bipolar-cycling fatigue in ferroelectric capacitors

Cite as: APL Mater. 9, 021113 (2021); doi: 10.1063/5.0038719

Submitted: 25 November 2020 • Accepted: 6 January 2021 •

Published Online: 9 February 2021





View Online



Export Citation



CrossMark

M. T. Do,^{1,2} N. Gauquelin,³  M. D. Nguyen,¹  F. Blom,⁴ J. Verbeeck,³  G. Koster,^{1,a)}  E. P. Houwman,^{1,b)} 
and G. Rijnders¹ 

AFFILIATIONS

¹MESA+ Institute for Nanotechnology, University of Twente, P.O. Box 217, 7500 AE Enschede, The Netherlands

²Hanoi National University of Education, 136 Xuan Thuy, Cau Giay, Hanoi, Vietnam

³Electron Microscopy for Materials Science, University of Antwerp, 2020 Antwerp, Belgium

⁴Canon Production Printing Netherlands, P.O. Box 101, 5900 MA Venlo, The Netherlands

Note: This paper is part of the Special Topic on 100 Years of Ferroelectricity—A Celebration.

Author to whom correspondence should be addressed: g.koster@utwente.nl

E-mail: e.p.houwman@utwente.nl

ABSTRACT

Polarization fatigue, i.e., the loss of polarization of ferroelectric capacitors upon field cycling, has been widely discussed as an interface related effect. However, mechanism(s) behind the development of fatigue have not been fully identified. Here, we study the fatigue mechanisms in Pt/PbZr_{0.52}Ti_{0.48}O₃/SrRuO₃ (Pt/PZT/SRO) capacitors in which all layers are fabricated by pulsed laser deposition without breaking the vacuum. With scanning transmission electron microscopy, we observed that in the fatigued capacitor, the Pt/PZT interface becomes structurally degraded, forming a 5 nm–10 nm thick non-ferroelectric layer of crystalline ZrO₂ and diffused Pt grains. We then found that the fatigued capacitors can regain the full initial polarization switching if the externally applied field is increased to at least 10 times the switching field of the pristine capacitor. These findings suggest that polarization fatigue is driven by a two-step mechanism. First, the transient depolarization field that repeatedly appears during the domain switching under field cycling causes decomposition of the metal/ferroelectric interface, resulting in a non-ferroelectric degraded layer. Second, this interfacial non-ferroelectric layer screens the external applied field causing an increase in the coercive field beyond the usually applied maximum field and consequently suppresses the polarization switching in the cycled capacitor. Our work clearly confirms the key role of the electrode/ferroelectric interface in the endurance of ferroelectric-based devices.

© 2021 Author(s). All article content, except where otherwise noted, is licensed under a Creative Commons Attribution (CC BY) license (<http://creativecommons.org/licenses/by/4.0/>). <https://doi.org/10.1063/5.0038719>

Ferroelectric materials have been used in many applications such as non-volatile ferroelectric random access memories^{1,2} and micro-electromechanical systems.³ However, these ferroelectric-based devices are often unstable after a prolonged operation under AC driving voltages. This is a consequence of the so-called polarization fatigue, i.e., the loss of polarization of the integrated ferroelectric capacitors upon bipolar field cycling. Polarization fatigue appears severe in ferroelectric capacitors with conventional metal electrodes such as Pt and Au, which are currently used in most of the devices.

Therefore, understanding of the physical mechanism(s) behind the development of fatigue is of great importance and may help improve the endurance of (metal-electrode) capacitors and thus the stability of the host devices.

Fatigued capacitors often show structural degradation.^{4–8} For example, with scanning electron microscopy (SEM), Balke *et al.*⁵ observed a molten PZT layer at the Pt/PZT interface in fatigued PZT ceramics. Also by SEM, Lou *et al.*^{6,7} observed delaminated spots in the Pt top electrode of fatigued PZT thin films. By Raman

spectroscopy, these authors found PbO, TiO₂, and pyrochlore materials inside the delaminated spots. Recently, by using time-of-flight second ion mass spectrometry (ToF-SIMS), Ievlev *et al.*⁸ observed Cu from the electrode to have diffused into the PZT structure in fatigued PZT thin films. All these data indicate that the development of polarization fatigue directly relates to an overall degradation of the metal/ferroelectric interface under field cycling.

To understand the mechanism(s) behind the polarization fatigue, one needs to understand the mechanisms behind (i) the microstructural degradation of the metal/ferroelectric interface during field cycling and (ii) the suppression of polarization switching in the cycled capacitor with degraded interfaces. These mechanisms have not been discussed satisfactorily.⁹ Balke *et al.*⁵ qualitatively explained that the interfacial molten PZT layer screens the external applied field, reducing the actual field seen by the remaining (ferroelectric) crystalline PZT layer, leading to an incomplete polarization switching in the cycled capacitor. However, they did not explain why the interfacial PZT structure becomes molten during field cycling. Furthermore, although their field screening model seems plausible, it needs further supporting evidence. Lou *et al.*¹⁰ proposed that there is significant electron injection from the metal into the ferroelectric layer during the field cycling and that these injected electrons can thermally decompose the ferroelectric lattice, leading to damaged non-functional areas. As a result, the number of available sites for reverse domain nucleation is significantly reduced, consequently suppressing the polarization switching of the cycled capacitor.⁷ The above scenarios seem to be plausible but need to be further experimentally verified. Ievlev *et al.*⁸ did not explain why Cu from the electrode can diffuse into the PZT layer during field cycling. These authors suggested that the PZT lattice becomes doped with Cu (during field cycling), showing a lower polarization compared to the (as-grown) bare PZT layer. However, we find this scenario implausible because the Cu diffusion was observed only nearby the Cu/PZT interface and the bulk of the PZT lattice in the cycled capacitor remained undisturbed.

Previously, we have shown that Pt/PbZr_{0.52}Ti_{0.48}O₃/SrRuO₃ (Pt/PZT/SRO) capacitors fabricated by pulsed laser deposition (PLD) show a fatigue onset at 10⁷–10⁸ bipolar field cycles.¹¹ Here, we identify the microscopic fatigue mechanism(s) of these devices. By scanning transmission electron microscopy (STEM), we clearly observe that the Pt/PZT interface becomes structurally degraded

after field cycling. The mechanisms of this interface degradation and the polarization switching suppression in the cycled capacitors are discussed in depth. These insights into the fatigue mechanisms provide important clues how to practically improve the endurance of (metal-electrode) ferroelectric capacitors.

The Pt/PbZr_{0.52}Ti_{0.48}O₃/SrRuO₃ (Pt-top/PZT/SRO-bottom) capacitors were grown on a TiO₂-terminated SrTiO₃ (STO) (001)-oriented substrate.¹² More details about the PLD growth conditions of the layers can be found in our previous work.¹¹ The ferroelectric properties were measured with an aixACCT TF-2000 analyzer. The fatigue behavior was investigated under square-bipolar electric field cycling. Small-signal capacitance–field (C–E) loops were measured by the aixACCT TF-2000 analyzer, with a slow scanning staircase DC bias superimposed with a low-field (2.6 kV/cm) 10 kHz AC modulation signal. In all electrical experiments, the bottom electrode was grounded. High Angle Annular Dark Field Scanning transmission electron microscopy (HAADF-STEM) and energy dispersive x-ray (EDX) spectroscopy were performed using the X-Ant-Em instrument operated at 300 kV at the University of Antwerp.

The capacitors become strongly fatigued under bipolar field cycles at various field amplitudes (E_{cy}) and cycling frequencies (f_{cy} ; Fig. 1). Here, the P–E loops were measured with a triangular field of 200 kV/cm and 1 kHz. The degree of fatigue after 10⁸ field cycles is slightly more severe under higher field amplitude. However, the fatigue onset occurs at approximately the same cycle number, of about 10⁷ cycles, under the investigated field from 120 kV/cm to 280 kV/cm. The degree of fatigue is almost independent of the cycling frequencies and depends only on the number of field cycles (n), in the investigated range.

The interface structures of a pristine and a 10⁹-field-cycle fatigued capacitor were characterized by cross-sectional STEM (Fig. 2). The pristine Pt/PZT interface is atomically sharp without any defective layer (the Pt lattice is not clearly visible due to an intentionally enhanced image contrast). However, the fatigued Pt/PZT interface shows some new features compared to the pristine interface: (i) a dark-contrast interfacial layer with a thickness from 5 nm to 10 nm and (ii) defective regions with unidentified structures extending to a depth of 30 nm–40 nm into the PZT layer. The PZT at larger depths is undisturbed and remains perfectly crystalline. Note that the epitaxial PZT/SRO bottom interface remains atomically sharp and unchanged during field cycling, similar to the interfaces of SRO/PZT/SRO capacitors.¹¹ The

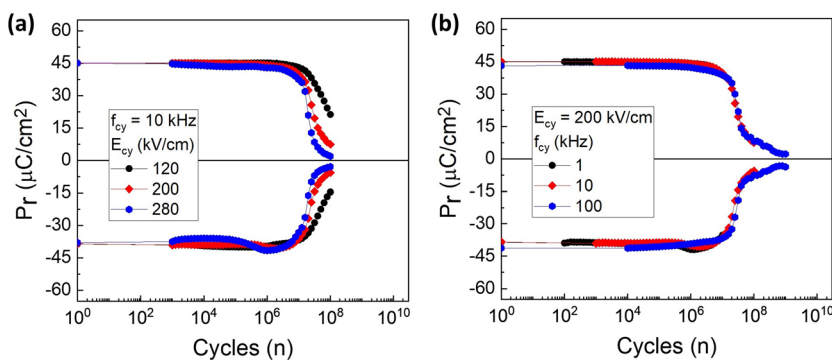


FIG. 1. Fatigue profiles of the capacitor under field cycling with various field amplitudes (a) and cycling frequencies (b). The P–E loops are measured with a triangular field of 200 kV/cm and 1 kHz.

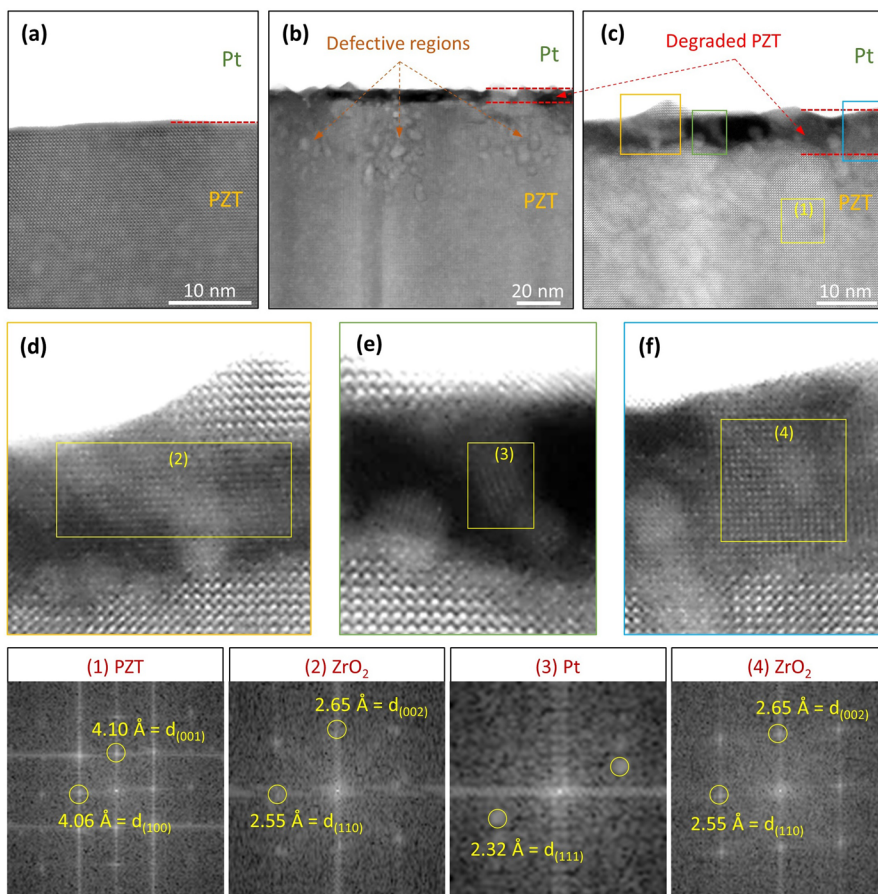


FIG. 2. STEM-HAADF investigation on the top Pt/PZT interface of the pristine (a) and fatigued capacitor [(b) and (c)]. [(d)–(f)] Zoomed-in images of different regions indicated by the colored boxes in (c). The bottom panels show FFT of regions marked by rectangle boxes (1–4).

dark-contrast interfacial layer at the Pt/PZT interface largely consists of nano-sized crystalline grains. The structures of these grains were determined by Fast Fourier Transform (FFT) on different regions marked by labeled boxes from (1) to (4) in Figs. 2(c)–2(f). Region 1 (inside the crystalline PZT) shows fringe spacings corresponding to the lattice parameters of the PZT lattice, $d_{(001)} \approx 4.10 \text{ \AA}$ and $d_{(100)} \approx 4.06 \text{ \AA}$ (ICSD 98-009-0478). Regions 2 and 4 (inside the interfacial layer) show similar FFT with fringe spacings of 2.65 \AA and 2.55 \AA , which are comparable with interplanar spacings of (002) and (110) planes of a ZrO_2 tetragonal structure (ICSD 98-000-9993), respectively, suggesting strongly that these are ZrO_2 grains. Region 3 (inside the interfacial layer) seems to be a Pt grain as its FFT fringe spacing of 2.32 \AA is equal to the spacing of Pt (111) planes (ICSD 98-004-1525).

Elemental maps obtained from energy dispersive x-ray spectroscopy (EDX) further confirm the structural changes in the Pt/PZT interface after field cycling (Fig. 3). The maps show a few nm thick transition boundary between the Pt and crystalline PZT layer. It is also clearly observed that Pt has diffused into this boundary layer, forming Pt-rich clusters. Furthermore, the concentrations of Pb, Zr, Ti, and O of the PZT vary along the interface and over the thickness of this boundary layer. Overall, our STEM

and EDX data show severe structural degradation of the PZT lattice near the Pt/PZT interface of the fatigued capacitor. Considering the presence of ZrO_2 and metallic Pt grains, it is reasonable to assume that the observed interfacial degraded layer is largely non-ferroelectric. Our data further confirm the previous reports on the ferroelectric structural degradation^{4–7} and the electrode material diffusion⁸ at the metal/ferroelectric interface in field-cycling fatigued capacitors.

The degradation of the capacitor microstructure leads to a change in the capacitance, confirmed by small-signal capacitance–field (C – E) measurements [see Fig. 4(a)]. The static capacitance of the pristine capacitor at 200 kV/cm , $C_0 \approx 100 \text{ pF}$, is much higher than that of the fatigued capacitor, $C_f \approx 65 \text{ pF}$. This decreasing trend is consistent with that reported in previous studies that fatigued Pt/PZT/Pt capacitors have lower capacitances than pristine capacitors.^{13,14} The fatigued capacitor can be modeled as two in-series connected capacitors: C_i of the interfacial degraded PZT layer and $C_{PZT/f}$ of the remaining crystalline ferroelectric PZT layer [see Fig. 4(b)]. One then has $\frac{1}{C_f} = \frac{1}{C_i} + \frac{1}{C_{PZT/f}}$, where $C_i = \frac{\epsilon_0 \epsilon_i A}{d_i}$ and $C_{PZT/f} = C_0 \frac{d_{PZT/p}}{d_{PZT/f}}$. Here, $d_{PZT/p} = 250 \text{ nm}$ is the thickness of the pristine PZT layer; d_i and ϵ_i are the average thickness and

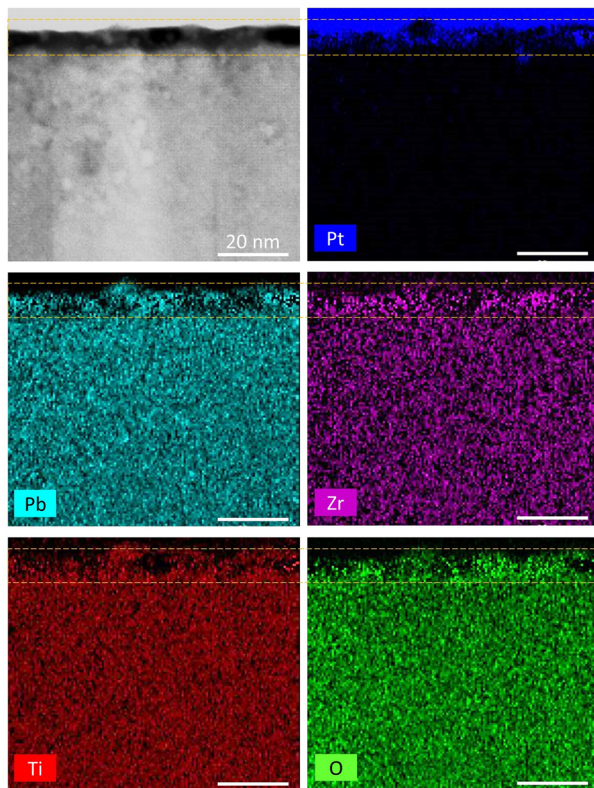


FIG. 3. Elemental maps of the fatigued Pt/PZT interface obtained from energy dispersive x-ray spectroscopy. The dashed lines highlight the interfacial layer of PZT with most degradation.

relative dielectric constant of the interfacial degraded PZT layer in the fatigued capacitor, respectively; $d_{PZT/f} = (d_{PZT/p} - d_i)$ is the thickness of the remaining crystalline PZT layer in the fatigued capacitor, and $A = 10^{-8} \text{ m}^2$ is the capacitor area. Estimating $d_i \approx 10 \text{ nm}$ from the STEM images, one obtains $\epsilon_i \approx 19$ (at the applied field of 200 kV/cm). This is a plausible dielectric constant value for the interfacial degraded PZT layer, which mostly consists

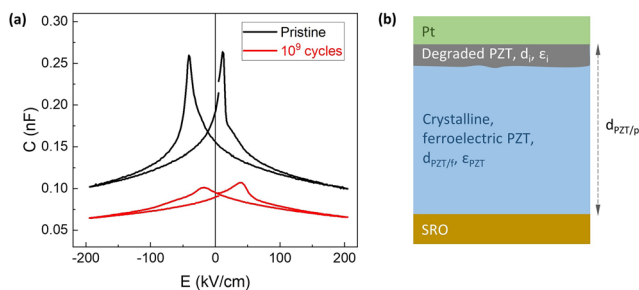


FIG. 4. (a) C–E loops of the pristine and 10^9 -cycle fatigued capacitor. (b) Schematic presentation of the fatigued capacitor consisting of an interfacial degraded non-ferroelectric layer and a remaining crystalline ferroelectric layer.

of non-ferroelectric ZrO_2 . Moreover, it is observed that the self-bias field disappears in the fatigued sample, indicating that the degraded interfacial layer diminishes the effect of the interface barrier.

The degradation of the Pt/PZT interface might be caused by the transient depolarization field, which appears during the nucleation of reverse domains under the bipolar field cycles, as previously suggested by Lou *et al.*¹⁰ The transient depolarization field E_{bc} at the interface is produced by unscreened positive bound charges ($\sigma \approx P_{PZT}$) on the top of the nucleating reverse domains and is directed from the PZT layer toward the electrode. The interfacial PZT layer suffers from this transient depolarization field once in every bipolar field cycle. In a simple approximation, E_{bc} at the interface is estimated as follows:

$$E_{bc} \approx \frac{\sigma}{\epsilon_0 \cdot \epsilon_{PZT}} \approx \frac{P_{PZT}}{\epsilon_0 \cdot \epsilon_{PZT}}. \quad (1)$$

With $P_{PZT} \approx 0.4 \text{ C/m}^2$ and $\epsilon_{PZT} \approx 300$, one obtains $E_{bc} \approx 1.5 \text{ MV/cm}$. This is higher than the reported DC breakdown field of many PZT films in the range of 0.6 MV/cm .¹⁵ Therefore, at a certain moment during the field cycling—in our devices after about 10^7 cycles—the top interfacial PZT lattice starts to decompose. The initial trigger of such structural decomposition might be an occurrence of a significant electron injection from the Pt electrode into the PZT layer, driven by the high transient depolarization field under the Fowler–Nordheim tunneling mechanism.¹⁰ Subsequently, the injected electrons with a high kinetic energy can locally heat the interface and thermally decompose the interfacial PZT, resulting in disordered materials, ZrO_2 grains, and a diffusion of Pt. The defective regions just below this severely degraded interfacial layer are also the consequence of this structural deterioration process. Note that the decomposition discussed here is a local effect, happening within the thin PZT layer adjacent to the interface. The remaining bulk PZT layer, further away from the interface, maintains its original perfect crystalline structure. This is different from the capacitor breakdown effect under a high external DC bias.¹⁵ In the later case, the broken capacitor normally appears with defective filamentary pathways, which form through the whole thickness of the ferroelectric layer, causing the capacitor to be electrically leaky or even conductive.

Generally, the field-assisted decomposition of a crystalline structure is strongly accelerated by the presence of defects. This explains why the (pristine) Pt/PZT top interface is much more sensitive to the decomposition than the epitaxial PZT/SRO bottom interface, despite the fact that both interfaces are exposed to the depolarization field under the same number of bipolar field cycles. At the PZT/SRO interface, the PZT lattice forms a strong chemical bond with the SRO lattice due to a continuous oxygen sub-lattice backbone.¹¹ In contrast, at the Pt/PZT interface, there is no such chemical bonding between the Pt and PZT lattices, so this interface is indeed a large planar lattice defect. Moreover, the deposition of Pt on the PZT surface reduces some of the Pb^{2+} into neutral metallic Pb.^{16–19} The Pt/PZT interface therefore contains compositional and lattice defects (which cannot be visualized from the above STEM images) due to the projection character of the technique and the thickness of the lamella. Due to these pre-existing defects, the field-assisted structural decomposition evolves much faster at the top Pt/PZT interface

compared to the bottom PZT/SRO interface. As a side note, the interfacial defects at metal/ferroelectric interface might also be the reason why metal-electrode capacitors show a lower DC breakdown strength than oxide-electrode capacitors.^{20,21}

As seen above, the fatigued capacitor after 10^9 cycles shows a 5–10 nm thick degraded layer adjacent to the Pt top electrode while the remaining PZT layer underneath is still crystalline. This crystalline PZT layer is expected to be ferroelectric. However, the measured polarization of the capacitor after 10^9 cycles is only about 10% of the pristine polarization (Fig. 1). We think that the maximum field of 200 kV/cm in the P–E loop measurements (as used in Fig. 1) is insufficient to completely switch the crystalline PZT layer in the cycled capacitor (from this point, called capacitor 1). To verify this, we fatigued another capacitor (called capacitor 2) using a same bipolar field cycling of 200 kV/cm and 100 kHz but measured its P–E loops with a maximum field of 800 kV/cm [see Fig. 5(a)]. From Fig. 5(b), the remnant-polarization fatigue profiles of these two capacitors are substantially different as capacitor 2 maintains the full polarization during field cycling. This indicates that the cycled capacitor, which has a degraded non-ferroelectric PZT layer at the top interface, requires a substantially higher applied field to attain polarization switching. This result also implies that the evolution profile of the remnant polarization under field cycling, which has commonly been used to represent the fatigue effect, is very sensitive to measurement parameters used to record the P–E loop.

P–E and I–E loops of the two capacitors are shown in Fig. 6. The P–E loops of capacitor 1 become suppressed and slanted with the increase in the field cycle number, corresponding to the depression of the switching peaks at ± 45 kV/cm in the I–E loops [Figs. 6(a) and 6(b)]. This leads to the usual conclusion that cycled ferroelectric capacitors become non-switchable. Differently, the P–E loops of capacitor 2 at different cycling states show a clear polarization-switching behavior, corresponding to prominent switching peaks in the I–E loops [Figs. 6(c) and 6(d)]. However, there are some major differences between the polarization switching of the cycled and the pristine capacitor, given as follows:

- (i) The capacitors after 2×10^7 – 3×10^7 cycles show a P–E loop with a double-step behavior [red and blue loops in Fig. 6(c)]. This is because their switching peaks at ± 45 kV/cm become suppressed, but new “fatigued” switching peaks appear at higher (absolute) field values [red and blue loops in Fig. 6(d)]. For example, after 2×10^7 cycles, the “fatigued” switching peaks appear at ± 170 kV/cm, and after 3×10^7 cycles, these peaks appear at ± 200 kV/cm. This behavior indicates that under field cycling, the capacitor became fatigued inhomogeneously, region-by-region. At further cycling, the current switching peaks of the “pristine” device at ± 45 kV/cm have almost completely disappeared and the “fatigued” switching peaks shift to higher field values, about ± 240 kV/cm after 10^8 cycles and ± 300 kV/cm after 10^9 cycles [pink and green loops in Fig. 6(d), respectively]. The P–E loops at these cycling states switch at a single higher coercive field, which suggests that the whole area of the capacitor has now become affected by the fatigue cycling process.
- (ii) The current switching peaks of cycled capacitors are broader than those of pristine devices. This is attributed to a broad range of switching fields (local coercive fields) in the fatigued regions of the capacitor. These data also imply that in the fatigued regions of the capacitor, the degree of fatigue varies between different locations.
- (iii) The “fatigued” switching peak under a positive applied field (when the Pt electrode is positively biased) is broader than the “fatigued” switching peak under a negative applied field (when the Pt electrode is negatively biased). This indicates that the polarization switching of upward-oriented domains (into downward-oriented domains) occurs over a more distributed applied field than the polarization switching of downward-oriented domains (into upward-oriented domains).

The ferroelectric data presented above indicate that the domain switching suppression in the cycled capacitor is caused by the degraded PZT layer at the Pt/PZT interface through the so-called field screening effect. The interfacial degraded PZT layer screens the

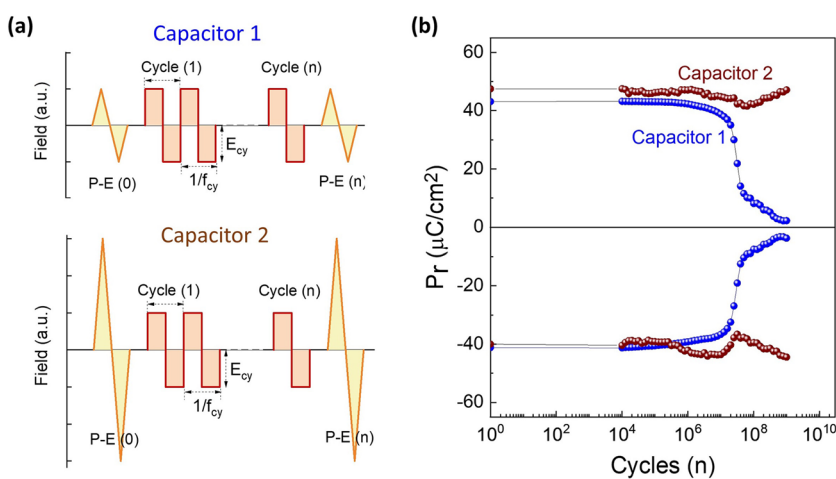


FIG. 5. (a) The field cycling (200 kV/cm at 100 kHz) for fatigue treatment is the same for both capacitors, but the P–E loops are measured with a maximum field of 200 kV/cm for capacitor 1 and 800 kV/cm for capacitor 2, respectively. (b) The obtained remnant-polarization profiles of the two capacitors.

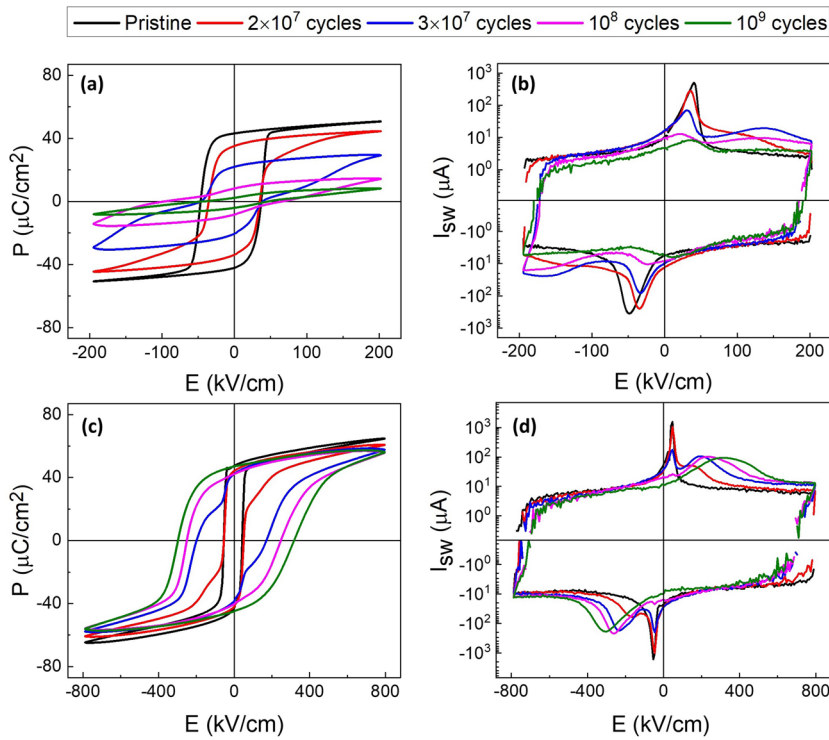


FIG. 6. P–E loops and I–E loops of capacitor 1 [(a) and (b)] and capacitor 2 [(c) and (d)] at different cycling states.

external applied field, reducing the actual field seen by the remaining (ferroelectric) crystalline PZT layer in the cycled capacitor and making the polarization switching incomplete. A similar mechanism was qualitatively discussed by Balke *et al.*⁵ Let us quantitatively model the field screening effect in our cycled Pt/PZT/SRO capacitor. The continuity of the displacement current across the dielectric layer/ferroelectric interface and the voltage drop across the two layers are given by

$$\epsilon_0 E_i + P_i = \epsilon_0 E_{PZT/f} + P_{PZT/f}, \quad (2)$$

$$E_i d_i + E_{PZT/f} d_{PZT/f} = E_{appl} d_{PZT/p}, \quad (3)$$

respectively, with E_i , $E_{PZT/f}$, and E_{appl} being the electric field in the interfacial degraded PZT layer, the remaining ferroelectric crystalline PZT layer, and the external applied field, respectively, and P_i and $P_{PZT/f}$ being the polarization of the degraded PZT layer and the remaining crystalline PZT layer, respectively. Because the interfacial degraded PZT layer is non-ferroelectric, we have $\epsilon_0 E_i + P_i = \epsilon_0 \epsilon_i E_i$. Therefore, from Eqs. (2) and (3), one obtains

$$E_i = \frac{E_{PZT/f}}{\epsilon_i} + \frac{P_{PZT/f}}{\epsilon_0 \epsilon_i}, \quad (4)$$

$$E_{PZT/f} = \frac{E_{appl} - \frac{P_{PZT/f}}{\epsilon_0 \epsilon_i} \frac{d_i}{d_{PZT/p}}}{\frac{1}{\epsilon_i} \frac{d_i}{d_{PZT/p}} + \frac{d_{PZT/f}}{d_{PZT/p}}} \approx E_{appl} - \frac{P_{PZT/f}}{\epsilon_0 \epsilon_i} \frac{d_i}{d_{PZT/p}}. \quad (5)$$

The last approximation applies for the considered devices in which $d_i \ll d_{PZT/f} \approx d_{PZT/p}$. From Eq. (5), it is seen that due to the interfacial dielectric layer, the field seen by the ferroelectric layer, $E_{PZT/f}$, is strongly reduced compared to the applied field, E_{appl} . At the moment when the remaining crystalline PZT layer in the cycled capacitor starts polarization switching, one would expect that $E_{PZT/f} \approx 45$ kV/cm (similar to the switching field of the pristine capacitor). Although the average effective polarization of the whole layer is zero (due to a pattern of oppositely oriented domains at the coercive fields in the P–E loop), the local polarization of the ferroelectric PZT material is $P_{PZT/f} \approx 40$ $\mu\text{C}/\text{cm}^2$. With these values, one obtains $E_i \approx 24.3$ MV/cm and $E_{appl} \approx 1.01$ MV/cm for the switching moment of the remaining crystalline PZT layer (in the cycled capacitor). It means that domain switching in the fatigued capacitor will occur if the externally applied field is above 1.01 MV/cm. This value is a few times higher than those observed from the P–E and I–E loops [in Figs. 6(c) and 6(d)] in the range 300 kV/cm–400 kV/cm. A possible reason is that we have just simply modeled the cycled capacitor as a series connection of only the degraded interfacial PZT layer and the remaining crystalline ferroelectric PZT layer and have not considered the contribution of the less deteriorated PZT layer (the defective regions) in between. The ferroelectricity and dielectric constant of this layer might be different from those of the crystalline PZT layer. However, the simple model above already shows the field screening effect caused by the interfacial degraded PZT layer, leading to a suppression of the domain switching of the cycled capacitor.

The results above suggest that ferroelectric capacitors with noble-metal electrodes always exhibit less fatigue-resistance than capacitors with oxide electrodes because of the ferroelectric/metal

interfaces with weak chemical bonding, which can be easily decomposed by the transient depolarization field during field cycling. Therefore, to improve the fatigue resistance, one needs to enhance the bonding between the electrode and the ferroelectric layer. This can be done by inserting a thin conductive oxide layer at the interface between the metal electrode and the ferroelectric layer.^{22–26} Another solution would be using a thin adhesion layer of Ti or Ta between the metal electrode and ferroelectric layer to form metal–metal bonding with the noble metal electrode on the one side and metal-oxide bonding with the ferroelectric layer on the other side, subsequently strengthening the capacitor interfaces. We believe that this is the main reason behind the favorable fatigue resistance of capacitors with Cu²⁷ and PtFe²⁸ electrodes.

In summary, we have experimentally identified the mechanisms behind the development of what used to be qualified as polarization fatigue in Pt/PZT/SRO thin-film capacitors fabricated by PLD but is, in essence, caused by a large increase in the coercive field. The Pt/PZT interface was observed to become structurally degraded, forming a non-ferroelectric layer of binary oxides and diffused Pt, after bipolar field cycling. This interface degradation is attributed to the cyclic occurrence of the transient depolarization field arising from the reverse domain nucleation under bipolar field cycles. The interfacial non-ferroelectric layer consequently screens the externally applied field, leading to a domain switching suppression in the cycled capacitor, shown up as a fatigue effect. These insights into the mechanisms behind the development of fatigue suggest a practical solution to improve the fatigue resistance of metal-electrode ferroelectric capacitors by enhancing the chemical bonding between the metal electrode and the ferroelectric layer.

This work was supported by the Nederlandse Organisatie voor Wetenschappelijk Onderzoek through Grant No. F62.3.15559. The Qu-Ant-EM microscope and the direct electron detector were partly funded by the Hercules fund from the Flemish Government. N.G. and J.V. acknowledge funding from the GOA project “Solarpaint” of the University of Antwerp. This work has also received funding from the European Union’s Horizon 2020 research and innovation program under Grant No. 823717—ESTEEM3. We acknowledge D. Chezganov for his useful insights.

DATA AVAILABILITY

The data that support the findings of this study are available from the corresponding author upon reasonable request.

REFERENCES

- 1 J. F. Scott and C. A. Paz de Araujo, *Science* **246**, 1400 (1989).
- 2 O. Auciello, J. F. Scott, and R. Ramesh, *Phys. Today* **51**(7), 22 (1998).
- 3 P. Murali, *J. Micromech. Microeng.* **10**, 136 (2000).
- 4 Y. Zhang, D. Lupascu, E. Aulbach, I. Baturin, A. Bell, and J. Rodel, *Acta Mater.* **53**, 2203 (2005).
- 5 N. Balke, H. Kungl, T. Granzow, D. C. Lupascu, M. J. Hoffmann, and J. Rödel, *J. Am. Ceram. Soc.* **90**, 3869 (2007).
- 6 X. Lou, X. Hu, M. Zhang, S. A. T. Redfern, and J. F. Scott, *Integr. Ferroelectr.* **73**, 93 (2005).
- 7 X. J. Lou, M. Zhang, S. A. T. Redfern, and J. F. Scott, *Phys. Rev. Lett.* **97**, 177601 (2006).
- 8 A. V. Ievlev, S. Kc, R. K. Vasudevan, Y. Kim, X. Lu, M. Alexe, V. R. Cooper, S. V. Kalinin, and O. S. Ovchinnikova, *Nat. Commun.* **10**, 3064 (2019).
- 9 A. K. Tagantsev, I. Stolichnov, E. L. Colla, and N. Setter, *J. Appl. Phys.* **90**, 1387 (2001).
- 10 X. J. Lou, M. Zhang, S. A. T. Redfern, and J. F. Scott, *Phys. Rev. B* **75**, 224104 (2007).
- 11 M. T. Do, N. Gauquelin, M. D. Nguyen, J. Wang, J. Verbeeck, F. Blom, G. Koster, E. P. Houwman, and G. Rijnders, *Sci. Rep.* **10**, 7310 (2020).
- 12 G. Koster, B. L. Kropman, G. J. H. M. Rijnders, D. H. A. Blank, and H. Rogalla, *Appl. Phys. Lett.* **73**, 2920 (1998).
- 13 J. J. Lee, C. L. Thio, and S. B. Desu, *J. Appl. Phys.* **78**, 5073 (1995).
- 14 R. Bouregba, N. Sama, C. Soyer, G. Poullain, and D. Remiens, *J. Appl. Phys.* **107**, 104102 (2010).
- 15 M. D. Nguyen, H. Yuan, E. P. Houwman, M. Dekkers, G. Koster, J. E. ten Elshof, and G. Rijnders, *ACS Appl. Mater. Interfaces* **8**, 31120 (2016).
- 16 M. Kurasawa and P. C. McIntyre, *J. Appl. Phys.* **97**, 104110 (2005).
- 17 Y. Chen and P. C. McIntyre, *Appl. Phys. Lett.* **91**, 072910 (2007).
- 18 F. Chen, R. Schafranek, S. Li, W. B. Wu, and A. Klein, *J. Phys. Appl. Phys.* **43**, 295301 (2010).
- 19 F. Chen, R. Schafranek, W. Wu, and A. Klein, *J. Phys. Appl. Phys.* **44**, 255301 (2011).
- 20 I. Stolichnov, A. Tagantsev, N. Setter, S. Okhonin, P. Fazan, J. S. Cross, and M. Tsukada, *J. Appl. Phys.* **87**, 1925 (2000).
- 21 X. Chen, Y. Zhang, B. Xie, W. Wang, M. Ding, and P. Yu, *J. Alloys Compd.* **831**, 154883 (2020).
- 22 T.-F. Tseng, R.-P. Yang, K.-S. Liu, and I.-N. Lin, *Appl. Phys. Lett.* **70**, 46 (1997).
- 23 X. D. Zhang, J. Dho, S. Park, H. Kwon, J. Hwang, G. Park, D. Kwon, B. Kim, Y. Jin, B. G. Kim, D. Karpinsky, and A. L. Kholkin, *J. Appl. Phys.* **110**, 064115 (2011).
- 24 H. Han, J. Zhong, S. Kotru, P. Padmini, X. Y. Song, and R. K. Pandey, *Appl. Phys. Lett.* **88**, 092902 (2006).
- 25 Y. Wang, F. Yuan, T. Wei, C. Zhu, K. F. Wang, Y. D. Xia, and J.-M. Liu, *J. Appl. Phys.* **101**, 016101 (2007).
- 26 K. Lee, B. R. Rhee, and C. Lee, *Appl. Phys. Lett.* **79**, 821 (2001).
- 27 D.-H. Do, P. G. Evans, E. D. Isaacs, D. M. Kim, C. B. Eom, and E. M. Dufresne, *Nat. Mater.* **3**, 365 (2004).
- 28 B. T. Liu, J. W. Zhao, X. H. Li, Y. Zhou, F. Bian, X. Y. Wang, Q. X. Zhao, Y. L. Wang, Q. L. Guo, L. X. Wang, and X. Y. Zhang, *Appl. Phys. Lett.* **96**, 252904 (2010).